J Digit Imaging (2012) 25:369–376
DOI 10.1007/s10278-011-9417-7

Evaluation of Texture for Classification of Abdominal Aortic Aneurysm After Endovascular Repair

Guillermo García · Josu Maiora · Arantxa Tapia · Mariano De Blas

Published online: 7 September 2011

Abstract The use of the endovascular prostheses in abdominal aortic aneurysm has proven to be an effective technique to reduce the pressure and rupture risk of aneurysm. Nevertheless, in a long-term perspective, complications such as leaks inside the aneurysm sac (endoleaks) could appear causing a pressure elevation and increasing the danger of rupture consequently. At present, computed tomographic angiography (CTA) is the most common examination for medical surveillance. However, endoleak complications cannot always be detected by visual inspection on CTA scans. The investigation on new techniques to detect endoleaks and analyse their effects on treatment evolution is of great importance for endovascular aneurysm repair (EVAR) technique. The purpose of this work was to evaluate the capability of texture features obtained from the aneurysmatic thrombus CT images to discriminate different types of evolutions caused by endoleaks. The regions of interest (ROIs) from patients with different post-EVAR evolution were extracted by experienced radiologists. Three techniques were applied to each ROI to obtain texture parameters, namely the grey level co-occurrence matrix (GLCM), the grey level run length matrix (GLRLM) and the grey level difference method (GLDM). The results showed that GLCM, GLRLM and GLDM features presented a good discrimination ability to differentiate between favourable or unfavourable evolutions. GLCM was the most efficient in terms of classification accuracy (93.41%±0.024) followed by GLRLM (90.17%±0.077) and finally by GLDM (81.98%±0.045). According to the results, we can consider texture analysis as complementary information to classified abdominal aneurysm evolution after EVAR.

Keywords Aneurysm · EVAR · Texture features · Neural network

G. García (✉) · A. Tapia
University of the Basque Country, Systems Engineering and Automatic Department, Polytechnical University College,
Plaza Europa 1,
20018 San Sebastian, Spain
e-mail: g.garcia@ehu.es

A. Tapia
e-mail: arantxa.tapia@ehu.es

J. Maiora
University of the Basque Country,
Electronics and Telecommunications Department,
Polytechnical University College,
Plaza Europa 1,
20018 San Sebastian, Spain
e-mail: j.maiora@ehu.es

M. De Blas
Interventional Radiology Department, Donostia Hospital,
Paseo Doctor José Beguiristain s/n,
20014 Donostia-San Sebastian, Spain
e-mail: mariano.deblasbravo@osakidetza.net

Introduction

The endovascular prostheses in abdominal aortic aneurysm have proven to be an effective technique to reduce the pressure and rupture risk of aneurysm, offering shorter post-operation recovery than open surgical repair. The endovascular aneurysm repair (EVAR) treatment is a percutaneous image-guided endovascular procedure in which a stent graft is inserted into the aneurysm cavity. Once the stent is placed, the blood clots around the metallic mesh forcing the blood flux through the stent and thus reducing the pressure on the aneurysm walls.

Nevertheless, in a long-term perspective, different complications such as prostheses displacement or leaks inside the aneurysm sac (endoleaks) could appear provoking a pressure elevation and increasing the danger of rupture consequently.

Due to this, periodic follow-up scans of the prosthesis behaviour are necessary. At present, contrast-enhanced computed tomographic angiography (CTA) is the most commonly used examination for imaging surveillance [1]. On the other hand, the post-operation analysis is quite crude as it involves manually measuring different physical parameters of the aneurysm cavity [2]. According to these measurements, the evolution of the aneurysm can be split up into two main categories:

- Favourable evolution. A reduction of the diameter of the aneurysm sac can be observed. This means that the aneurysm has been correctly excluded from the circulation.
- Unfavourable evolution. A growth of the aneurysm diameter in the presence of endoleaks is observed. Endoleaks can be detected thanks to contrast in the CT images.

The time series of CTA images of two patients who underwent EVAR treatment and experimented favourable or unfavourable evolution are shown in Fig. 1.

We could also distinguish a subcategory inside the unfavourable evolution cases. There are patients in which abdominal aneurysm does not increase or reduce significantly its volume and endoleaks are not visually detected (endotensión). Even today the cause for this behaviour remains a source of controversy [3].

Initially, the study has been focused on the former main categories, favourable and unfavourable. The principal hypothesis behind the study is that texture thrombus in favourable shrinking aneurysms might differ from unfavourable expanding ones so texture parameters could be used as complementary information. If the hypothesis is confirmed, we consider the extension of the analysis to endotension cases in posterior studies. Finally, we envision a decision support system based on texture features which might provide clinicians with complementary information for correctly classifying EVAR evolution. This is clinically important because a more complete assessment of EVAR progression would be useful in redefining management pathways for patients, particularly when new treatment options are available [4].

Texture Analysis

In recent years, many efforts have been put into the developing of Computer-Aided Diagnosis (CAD) systems

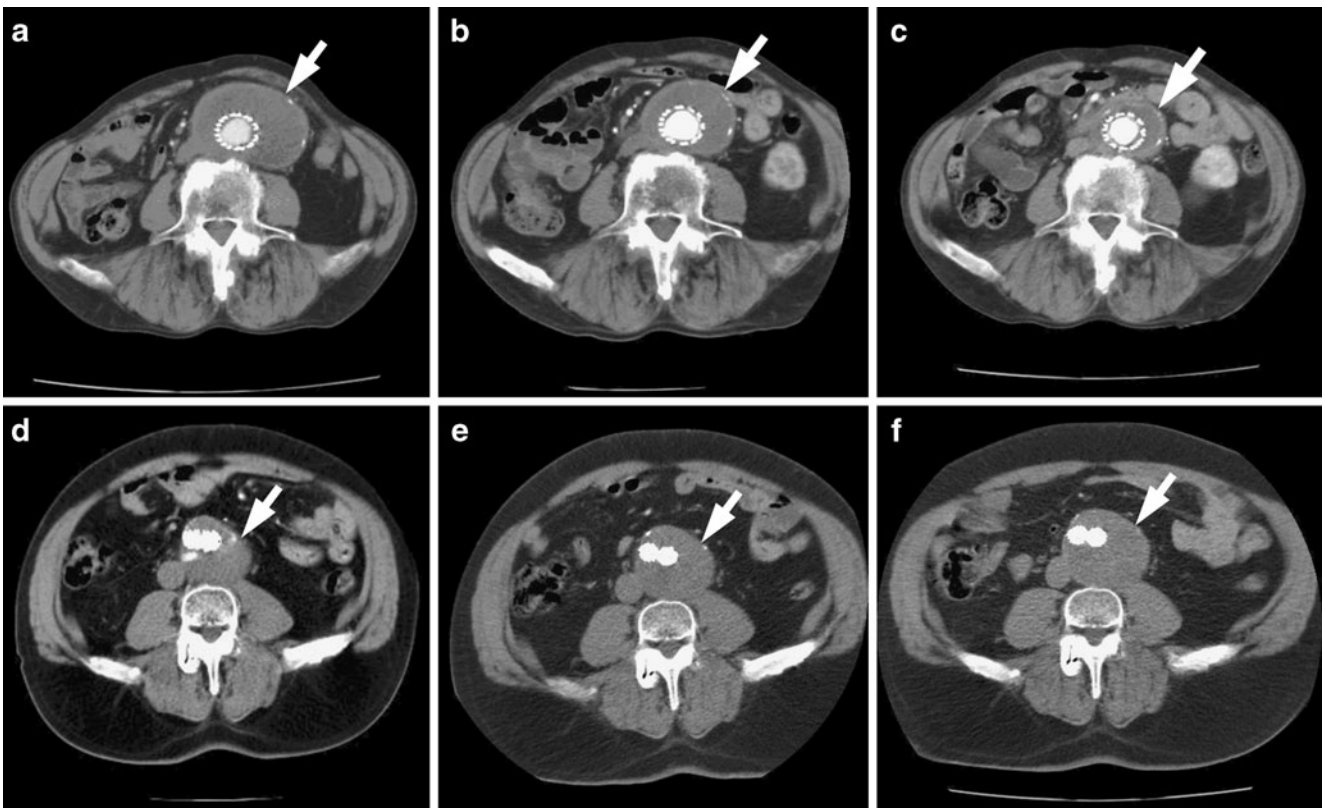

Fig. 1 CTA images of two patients treated with EVAR. *Top row* favourable evolution—**a** 1 year after treatment, **b** 2 years after treatment, and **c** 3 years after treatment. *Bottom row* unfavourable evolution—**d** 1 year after treatment, **e** 2 years after treatment, and **f** 3 years after treatment. *White arrow* points aneurysm sac in all of the scans

based on image processing methods. The principal motivation for the research on this kind of systems has been to assist the clinicians on the analysis of medical images [5, 6]. In many occasions, this analysis implies the detection or measurement of subtle differences, usually difficult to appreciate by visual inspection even for experienced radiologist.

CAD systems have been successfully utilized in a wide range of medical applications, mainly on the cancer detection and diagnosis field [7–9] but also in areas as diagnosis of osteoporosis [10], neuroimaging to detect lesions and abnormalities [11], or the detection of intracranial aneurysms [12].

A particular field inside the image processing methods is the so-named texture-based analysis. This analysis studies not only the variation of the pixel intensity values along the image, but also the possible spatial arrangement of them and the more or less periodic repetition of such arrangement (primitives). From this point of view, texture analysis can help on the functional characterization of different kind of organs, tissues, etc. at the evolution of disease. The texture features obtained from the analysis can be fed as inputs for a deterministic or probabilistic classifier, which assign each sample with its specific class.

Texture analysis methods can generally be classified into three categories: statistical methods, model-based methods, and structural methods [13]. In our approach we have focused on the application of statistical texture methods, specifically, on spatial domain statistical techniques as the grey level co-occurrence matrix (GLCM) [14], the grey level run length matrix (GLRLM) [15, 16], and the grey level difference method (GLDM) [17, 18]. These three very extended methods can capture second or higher order statistics on the relation between grey values in pixel pairs or groups of pixels in order to estimate their probability-density functions. Their validity has been proved in many studies. Mir et al. [19] utilized spatial grey level dependence matrix (SGLDM), GLRLM, and GLDM to detect abnormalities in CT images. Chen et al. [20] used GLCM texture features as inputs for a probabilistic neural network for the classification of hepatic tissue. In [21], Kim et al. analysed the use of SGLDM, GLRLM, and GLDM for the detection of microcalcifications in digitized mammograms. Vince et al. [22] compared five texture analysis techniques (first-order statistics, Haralick's method, Laws' texture energy method, the neighbourhood grey-tone difference matrix method, and texture spectrum features) in characterization of coronary plaques on intravascular ultrasound images and found that the GLCM method established the most accurate results. Gibbs et al. [23] reported significant differences in the GLCM texture of benign and malignant lesions in the breast MRI. In Valavanis et al. [24], SGLDM and GLDM were used for obtaining texture features from hepatic tissue non-enhanced CT images and applied to a backpropagation neural network which classified them in four categories.

Our purpose in this study is to investigate the GLCM, GLRLM, and GLDM capacity for the discrimination between favourable and unfavourable evolutions of patients after abdominal EVAR treatment. For obtaining this objective, a semi-automated segmentation process to facilitate the extraction of samples has been developed. Once the samples from patients with different post-EVAR evolution have been obtained, the texture features from the three methods are calculated and fed into a feed-forward neural network classifier for automatic classification.

The paper is organised as follows: the "Materials and Methods" section provides information about the acquisition of CTA images, the description of the segmentation process, the theoretical background on the texture analysis methods, and the definition of neural network structure. The methodology and results obtained from the performance evaluation of the classifier are presented in the "Results" section. Finally, some conclusions are given in the "Conclusion" section.

Materials and Methods

Dataset

The CTA image scans used in this work were obtained by a group of three experienced radiologists from the Vascular Surgery Unit and Interventional Radiology Department of the Donostia Hospital. These CTA images belong to the scan studies of 70 patients with ages ranging from 70 to 93 years, conducted over a maximum of 5 years in fixed periods of 6–12 months.

The total patient set was selected by each one of the radiologist, unaware of each others' results. The criteria for unfavourable evolution cases were based on the detection of contrast medium within the aneurysm sac or on a regular increase in aneurysm diameter. For each data point, the changes in diameter were determined by subtracting follow-up measurements from preoperative measurements. Anterior–posterior aneurysm diameter measurements were obtained from CT slices orthogonal to the aortic axis and only diameter changes ≥2 mm were considered significant. For favourable cases, the criteria were based on the absence of contrast and on a stable reduction of aneurysm diameter during the entire follow-up. In order to generate ground-truth data sets, only cases with complete agreement on classification among all radiologists were selected. Balanced sample sets for training and testing the classifier system were obtained. A total of 35 CTA studies belonged to the "favourable evolution" class and 35 to the "unfavourable" one. All the studies were taken from the

abdominal area with a spatial resolution of 512×512 pixels and 12-bit grey level at the WW400 and WL40 window and 5 mm in thickness in DICOM format. For each patient, a maximum of three regions of interest (ROIs) (15×15 pixels) from aneurysm thrombus were manually extracted from different slices by radiologists, resulting in a total of 210 ROIs. Half of them corresponded to the "favourable evolution" group and the rest to the "unfavourable" one.

Segmentation Process

In order to facilitate the extraction of samples by radiologists, a semi-automated segmenting process of the aneurysm has been implemented. We used ITK [25] and VTK [26] open-source software toolkits as a base for the implementation of the process. Initially, meta-images were created from computerized tomography slices in DICOM format. During the process, the resolution and the spacing of the original images were preserved. The files obtained were used as inputs for the following 3D processing pipeline. First, a segmentation process of anatomical structures (spinal canal, lumen, and thrombus) is carried out. We have used a User-Guided Level Set Segmentation (UGLSS) [27] based on the 3D active contour segmentation method called region competition to get the segmented image of the spinal canal, lumen, and thrombus. It is a semi-automatic method that suits well in cases where the boundaries of the structure of interest are not well defined due to similar grey level values of surrounding tissues. The UGLSS algorithm proceeds as follows: First, the image is resampled into a volume with isotropic spacing (1,1,1). Then, the regions of interest which contains a structure to segment are selected sequentially. The spinal canal in the first case, the lumen (stent graft) in the second case, and finally the thrombus are selected. During the preprocessing, the probability maps are computed by applying a smooth lower and upper threshold. The algorithm includes confidence connected voxels that lie in an interval of the current segmented region in an iterative process [28]. Finally, we place a spherical seed to initialize an evolving contour and we establish the parameters that control the propagation and curvature velocity. The evolving contour is a closed surface $C(t,u,v)$ parameterized by variables u, v, and by the time variable t [29]. The contour evolves according to the following partial differential equation:

$$\frac{\partial}{\partial t} C(t,u,v) = F\vec{N} \tag{1}$$

Where F is an external force incorporating information from the image being segmented and acting on the contour in the normal direction N. We compute the external force F by estimating the probability that a voxel belongs to the structure of interest (P_{obj}) and the probability that it belongs to the background (P_{bg}) at each voxel in the input image:

$$F = \alpha(P_{\mathrm{obj}} - P_{\mathrm{bg}}) + \beta K \tag{2}$$

Where K is the mean curvature of the contour, and α and β are weights that modulate the relative contribution of the two components of F [30]. As the method is semi-automatic, we stop the execution of the algorithm when we consider that the contour is corresponding to the structure we are interested in. Manual erosion was necessary on some occasions to remove imperfections during the thrombus segmentation process. The segmented volume is resliced along the axial plane facilitating the extraction of thrombus aneurysm samples by specialists. An example of the 3D processing pipeline result is shown in Fig. 2.

Texture Analysis—Feature Extraction

Grey Level Co-ocurrence Matrix

The GLCM [14] is an estimation of a second order joint conditional probability-density function $f(i,j/d,\theta)$. This function characterizes the spatial interrelationships of the grey values in an image. The values of the co-occurrence matrix elements represent the probability of going from grey level i to grey level j given that they are separated by the distance d and the direction is given by the angle θ (usually θ=0°, 45°, 90°, and 135°). For computing this probability, the image is scanned in direction θ and the co-occurrences accumulated in the GLCM. GLCM features are extracted for '$n\times n$' primitive template matrix in the directions 0°, 45°, 90°, and 135°, and in some cases, averaging is done to make them direction invariant.

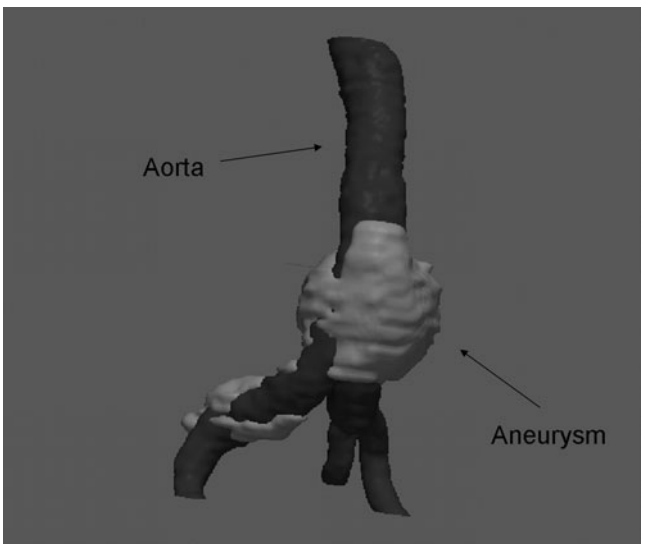

Fig. 2 3D view of a segmented aneurysm (*light colour*) and aorta volume (*dark colour*)

In the present application, GLCM features have been calculated at distance 1 due to the reduced size of the aneurysm samples. Initially, the assumption of an isotropic texture distribution inside the aneurysm sac was considered, consequently averaging over the four angular directions was computed. To reduce the influence of random noise on texture features, the number of grey levels was reduced to 16 prior to the accumulation of the matrix.

From GLCM matrix, a set of features are obtained to classify the kind of texture analysed. In this study, 13 features have been evaluated: energy, correlation, inertia, entropy, inverse difference moment, sum average, sum variance, sum entropy, difference average, difference variance, difference entropy, and two information measures of correlation.

The Grey Level Run Length Matrix

The GLRLM [15] is a way of extracting higher order statistical texture information. For a given image, a run length matrix is a two-dimensional matrix in which each element $p(i,j/\theta)$ represents the total number of runs with pixels of grey value i and run length j in a certain direction θ. The number of grey levels in the image is usually reduced by re-quantization before the accumulation of the matrix. Averaging over the four angular directions was computed and the number of grey levels has been kept in 16, equal than in the GLCM method in order to make both methods comparable.

Various texture features can then be extracted from the run length matrix. In our case the following 11 features has been calculated: short run emphasis, long run emphasis, grey level nonuniformity, run length nonuniformity, run percentage, low grey level run emphasis, high grey level run emphasis, short run low grey level emphasis, short run high grey level emphasis, long run low grey level emphasis, and long run high grey level emphasis.

Grey Level Difference Method

The GLDM [17] is a way of obtaining first-order statistics of local property values. The GLDM is based on the occurrence of two pixels which have a given absolute difference in grey level and which are separated by a specific displacement δ. Let $g(x,y)$ represent the digital picture function. For any given displacement vector $\delta=(\Delta x,\ \Delta y)$, where x and y are integers, let $g_\delta(x,y) = |g(\Delta x,\ \Delta y) - g(x+\Delta x, y+\Delta y)|$ and $D(i/\delta)$ be the estimated probability-density function defined by the expression:

$$D(i/\delta) = P(g_\delta(x,y) = i) \quad (3)$$

In this analysis, four possible forms of the vector δ will be considered: (0, d), ($-d$, d), (d, 0), and (d, $-d$) where d is the intersample spacing distance. Due to the reduced size of the aneurysm samples, d distance was considered equal to 1. Five textural features are measured from $D(i/\delta)$: contrast, angular second moment, entropy, mean, and inverse difference moment [18]. As with the GLCM method, the assumption of an isotropic texture distribution inside the aneurysm sac was considered, consequently averaging over the four angular directions was computed.

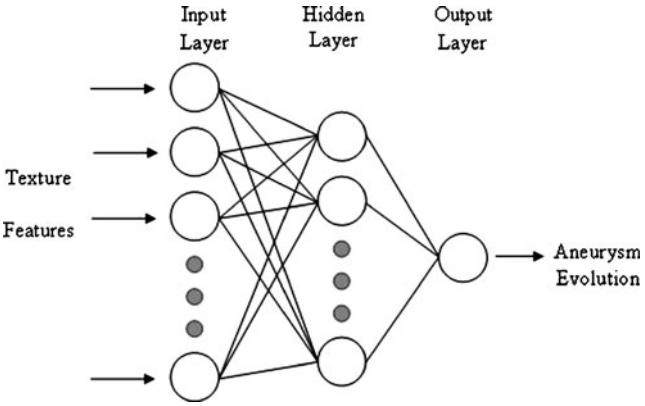

Fig. 3 Schematic of the artificial neural network (ANN) used as a classifier

Classification

The type of classifier employed in this research was a three-layer backpropagation neural network [31, 32]. The structure for this neural network consisted of an input layer with a number of input neurons equal to the number of features of the used set, one hidden layer with a variable number of neurons, and an output layer with one neuron. A nonlinear sigmoid function with zero and one saturation values is used as the activation function for each neuron, both the hidden layer and the output layer. The network is trained to provide a 0.9 output value for a favourable evolution sample and a 0.1 output value for an unfavourable evolution one. Figure 3 shows a schematic of the artificial neural network used as a classifier in this work.

Three neural networks with different number of input nodes were implemented. A neural network with 13 input nodes for GLCM, another with 11 input nodes for GLRLM,

Table 1 The average classification accuracy (in %) for training and testing sets of the neural network is given for the GLCM, GLDM, and GLRLM features

Texture method	Accuracy (%)—training		Accuracy (%)—testing	
	Mean	SD	Mean	SD
GLCM	94.46	0.003	93.41	0.024
GLDM	91.41	0.007	90.17	0.077
GLRLM	82.05	0.047	81.98	0.045

Table 2 The AUC values (mean±standard deviation) calculated for feature training and testing sets using the tenfold cross validation

Texture method	AUC_mean—training		AUC_mean—testing	
	Mean	SD	Mean	SD
GLCM	0.981	0.003	0.977	0.023
GLDM	0.976	0.003	0.960	0.022
GLRLM	0.868	0.004	0.851	0.028

and another one with 5 input nodes for GLDM. All the textural features were normalized by the sample mean and standard deviation of the data set before being fed to the neural network. The backpropagation algorithm with adaptive learning rate and momentum [31] was used for neural networks training. In order to find the appropriate number of hidden neurons, and the values of learning rate and momentum for each neural network, a trial-and-error process was applied. Finally a hidden layer of 20 neurons was found appropriate for all neural networks.

To evaluate the network performance during the training and testing process, the criterion was the mean square error given in Eq. (4)

$$\mathrm{MSE} = \frac{1}{N}\sum_{i=1}^{N}(o_i - t_i)^2 \tag{4}$$

where o_i and t_i are the output value and the target value for the ith input pattern, respectively, and N is the total number of training patterns. The training process is stopped when the MSE error no decreases for a significant number of iterations or when it starts increasing.

Results

In order to evaluate the potential of texture analysis to discriminate between the two types of aneurysm evolution, the development and validation of the neural network have been based on the tenfold cross validation method [32]. The 210 texture feature data sets were randomised and divided into 10 sets of 21 samples each. The neural networks were trained and tested with each one of the ten sets. Each time, nine of the sets were used for training the net and the remaining one was used for testing. To improve the evaluation of performance of the feature sets, the tenfold cross validation was repeated six times averaging the results.

The average of total percent of correctly classified cases (accuracy) for all the trials was used as an estimate of the performance of each classifier and consequently of the discrimination ability of textures features for differentiate between favourable or unfavourable cases. Table 1 shows the accuracy values (mean±standard deviation) estimated by the 10-fold cross validation of the training and testing sets of each texture analysis method.

From the Table 1, it is shown that all texture analysis methods supplied the neural network with enough discriminative information to differentiate between aneurysm

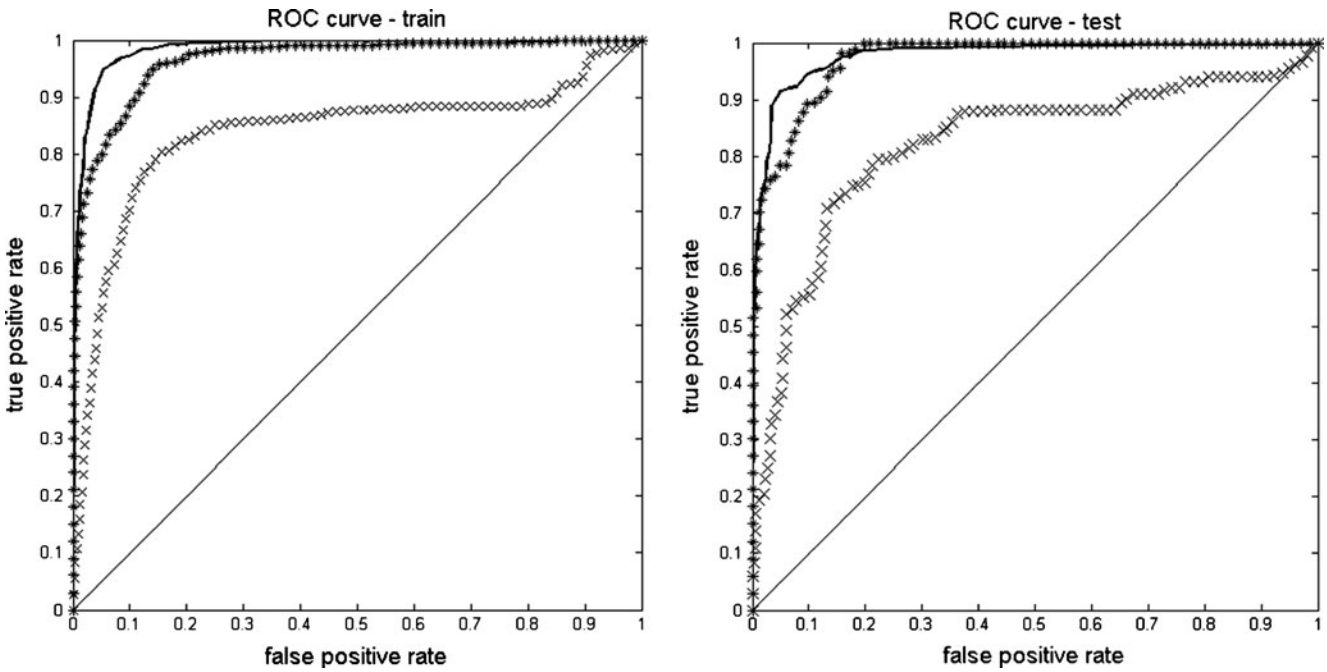

Fig. 4 Averaged ROC curves for training (*left*) and testing (*right*) sets from GLCM (*line*), GLDM (*asterisk*), and RLGM (*multiplication sign*) features fed into neural network inputs

evolutions. The best performing features set in terms of correctly classified cases corresponds to the GLCM method (93.41%±0.024) but the other two methods, GLDM (90.17%±0.077) and GLRLM (81.98%±0.045), could also be considered as significant.

The area under the ROC curve (AUC) was also used as a measure of the classification performance. Table 2 presents the AUC values (mean±standard deviation) calculated for feature training and testing sets using the tenfold cross validation.

The obtained values show again that the biggest area under the ROC curve, and consequently the best performance of the classifier is obtained with the set of features extracted with the GLCM method (AUC=0.977±0.023), followed by the GLDM (AUC=0.960±0.022), and the GLRLM methods (AUC=0.851±0.028). Figure 4 depicts the average ROC curves obtained using the tenfold cross validation testing sets for each texture method.

Although the GLCM method scores the highest AUC value, the GLDM method follows it very closely. The GLRLM method performance is the worst of the three but it can still be considered as indicative. These ROC curves confirm the previous accuracy results and reinforce the hypothesis of using texture analysis as discriminative information.

According to the classification accuracy and area under ROC curve results for the three methods, we could affirm that texture analysis might offer complementary information to support radiologist on classifying aneurysm evolution after EVAR.

Conclusions

In the present study, we have analysed the discriminative capacity of textures features for classifying the evolution experimented by aorta aneurysm treated by EVAR. For this purpose, texture parameters have been extracted by three different methods, GLCM, GRLM, and GLDM. The texture feature set obtained by each method was separately fed to an artificial neural network classifier. The classification performance of the three texture analysis methods were evaluated by percent of correctly classified cases and area under the ROC curve values estimated by the tenfold cross validation.

The results obtained by each texture analysis method permit to assert that the two main aortic thrombus aneurysm evolutions, namely favourable or unfavourable, correspond to different textures parameters. Consequently, we can conclude that texture analysis could be utilized by physicians as complementary information to classify the post-operative evolution in patients who underwent EVAR treatment.

The results can be considered as promising, taking into account the limited number of patients. A bigger patient dataset would be needed in order to generalise the findings to different clinical situations. The study can also be regarded as a first step to more specific studies, particularly for the unfavourable endotension cases. In these cases a better knowledge of the specific reasons that provokes the leakage from prosthesis to the aneurysmatic sac could be precious at the time to decide the treatment to follow.

References

1. Thompson MM: Controlling the expansion of abdominal Aneurysm. Br J Surg 90:897–898, 2003
2. VanDamme H, Sakalihasan N, Limet R: Factors promoting rupture of abdominal aortic aneurysms. Acta Chir Belg 105(1):1–11, 2005
3. Stavropoulos SW, Charagundla SR: Imaging Techniques for Detection and Management of Endoleaks after Endovascular Aortic Aneurysm Repair. Radiology 243:641–655, 2007
4. Bashir MR, Ferral H, Jacobs C, McCarthy W, Goldin M: Endoleaks After Endovascular Abdominal Aortic Aneurysm Repair: Management Strategies According to CT Findings. Am J Roentgenol 192:W178–W186, 2009
5. Doi K: Computer-aided diagnosis in medical imaging: Historical review, current status and future potential. Comput Med Imaging Graph 31(4–5):198–211, 2007
6. Duncan JS, Ayache N: Medical image analysis: Progress over two decades and the challenges ahead. *IEEE Trans. Pattern Anal. Mach. Intell.* 22:85–106, 2000
7. Viborny CJ, Giger ML, Nishikawa RM: Computer aided detection and diagnosis of breast cancer. Radiol Clin N Am 38(4):725–740, 2000
8. Morton MJ, Whaley DH, Brandt KR, Amrami KK: Screening mammograms: interpretation with computer-aided detection-prospective evaluation. Radiology 239:375–383, 2006
9. Li H, Wang Y, Liu KJ, et al: Computerized radiographic mass detection—part I. Lesion site selection by morphological enhancement and contextual segmentation. IEEE Trans Med Imag 20:289–301, 2001
10. Genant HK, Wu CY, Van KC, Nevitt MC: Vertebral fracture assessment using a semiquantitative technique. J Bone Miner Res 8:1137–1148, 1993
11. Boniha L, Kobayashi E, Castellano G, Coelho G, Tinois E, Cendes F, et al: Texture analysis of hippocampal sclerosis. Epilepsia 44:1546–1550, 2003
12. Arimura H, Li Q, Korogi Y, Hirai T, Abe H, Yamashita Y, Katsuragawa S, Ikeda R, Doi K: Automated computerized scheme for detection of unruptured intracranial aneurysms in threedimensional MRA. Acad Radiol 11:1093–1104, 2004
13. Zhang J, Tan T: Brief review of invariant texture analysis methods. Pattern Recognit 35(3):735–747, 2002. ISSN 0031–3203
14. Haralick R, Shanmugam K, Dinstein I: Textural features for image classification. IEEE Trans Syst Man Cybern SMC-3:610–621, 1973
15. Galloway RMM: Texture analysis using gray level run lengths. Comput Graph Image Process 4:172–179, 1975
16. Chu A, Sehgal CM, Greenleaf JF: Use of gray value distribution of run lengths for texture analysis. Pattern Recognit Lett 11:415–420, 1990
17. Weszka JS, Dyer CR, Rosenfeld A: A comparative study of texture measures for terrain classification. IEEE Trans Syst Man Cybern SMC-6:269–285, 1976

18. Conners RW, Harlow CA: A theoretical comparison of texture algorithms. IEEE Trans Pattern Anal 2:204–222, 1980
19. Mir AH, Hanmandlu M, Tandon SN: Texture analysis of CT images. Eng Med Biol Mag IEEE 14(6):781–786, 1995
20. Chen EL, Chung P-C, Chen CL, Tsa HM, Chang CI: An automatic diagnostic system for CT liver image classification. IEEE Trans Biomed Eng 45(6):783–794, 1998
21. Kim JK, Park HW: Statistical textural features for detection of microcalcifications in digitized mammograms. Med Imaging IEEE Trans 18(3):231–238, 1999
22. Vince DG, Dixon KJ, Cothren RM, Cornhill JF: Comparison of texture analysis methods for the characterization of coronary plaques in intravascular ultrasound images. Comput Med Imaging Graph 24:221–229, 2000
23. Gibbs P, Turnbull LW: Textural analysis of contrast-enhanced MR images of the breast. Magn Reson Med 50:92–98, 2003
24. Nikita A, Nikita KS, Mougiakakou SG, Valavanis IK. In: Evaluation of Texture Features in Hepatic Tissue Characterization from Non-Enhanced CT Images. Engineering in Medicine and Biology Society, 2007. EMBS 2007. 29th Annual International Conference of the IEEE, 2007, p 3741–37414
25. Ibanez L, Schroeder W: The ITK Software Guide. Kitware, Inc. ISBN 1-930934-10-6, http://www.itk.org/ItkSoftwareGuide.pdf, 2003
26. VTK: The visualization toolkit. http://www.vtk.org
27. Yushkevich PA, Piven J, Hazlett HC, Smith RG, Ho S, Gee JC, Gerig G: User-guided 3D active contour segmentation of anatomical structures: Significantly improved efficiency and reliability. Neuroimage 31:1116–1128, 2006
28. Caselles V, Kimmel R, Sapiro G: Geodesic active contours. Int J Comput Vis 22(1):61–97, 1997
29. Sethian J: Level Set Methods and Fast Marching Methods. Cambridge University Press, 1996
30. Zhu SC, Yuille A: Region competition: unifying snakes, region growing, and Bayes/mdl for multiband image segmentation. IEEE Trans Pattern Anal Mach Intel 18(9):884–900, 1996. ISSN 0162-8828
31. S Haykin: Neural networks: A Comprehensive Foundation. Prentice-Hall, 1999
32. Weiss SM, Kulikowski CA: Computer systems that learn: Classification and prediction methods from statistics, neural nets, machine learning, and expert systems. Morgan Kaufmann, San Mateo, 1991